Supporting Information

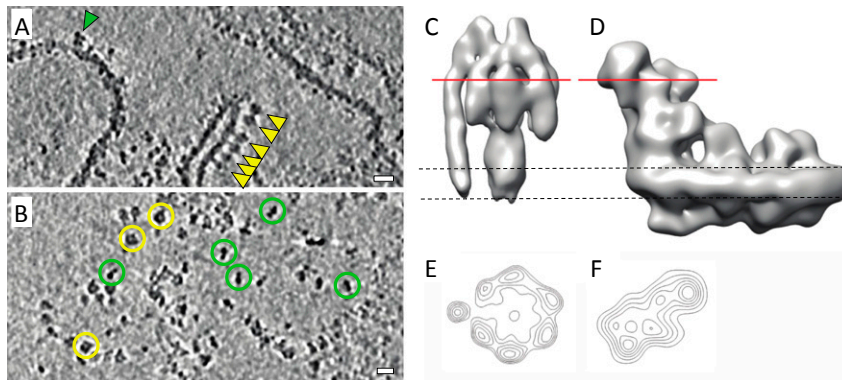## Davies et al. 10.1073/pnas.1720702115

Fig. S1. ATP synthase and complex I in tomographic volumes. (*A* and *B*) Slices through tomographic volumes of bovine heart mitochondrial membranes indicating side views (*A*) and matrix views (*B*) of ATP synthase (yellow arrowheads and circles) and complex I (green arrowhead and circles). (*C*) Subtomogram average of ATP synthase at ∼25 Å resolution (EMD-2982). (*D*) Single-particle average of complex I Fourier-filtered to ∼25 Å resolution (EMD-2676). (*E* and *F*) Cross-sections through *C* and *D* at the level of the red line indicate density profiles of ATP synthase (*E*) and complex I (*F*) 100 Å above the membrane (dashed line). (Scale bars: 20 nm.)
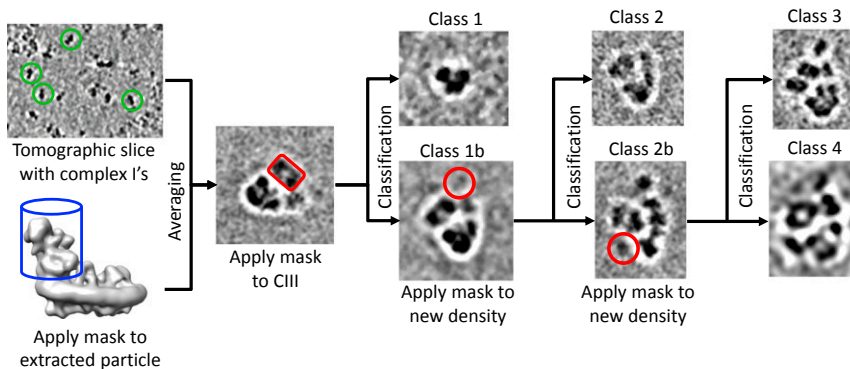
Fig. S2. Averaging and classification. Complex I densities were identified in tomographic volumes by the bar-shaped appearance of the matrix domain (green circles). A cylindrical mask (blue) was applied to exclude other densities from the alignment. After averaging, subvolumes were classified according to the presence of neighboring densities (red box and circles). For bovine heart and *Y. lipolytica*, three rounds of classification were performed, resulting in four classes. Only one round of classification was required for *A. officinalis*.

Fig. S3. Subtomogram averages and atomic models of complex III_2 and complex IV_1. (*A*) Different views of complex III_2. (*B*) Complex III_2 Fourier-filtered to 40 Å resolution (PDB ID code 1BCC) (10). (*C*) Density extracted from subtomogram average of complex III_2. (*D*) Different views of the atomic model of complex IV_1 (PDB ID code 1OCC) (7). (*E*) Atomic model of complex IV_1 rendered to 40 Å resolution. (*F*) Density of complex IV_1 extracted from subtomogram average.

Fig. S4. Comparison of bovine subtomogram average with single-particle cryo-EM structures. Atomic models derived by single-particle cryo-EM (24, 25, 27, 28, 38) were Fourier-filtered to 40 Å and aligned to the subtomogram average on complex I (blue). Complex positions are outlined. Both complex III_2 and complex IV_1 show some degree of positional variability relative to complex I. In one single-particle structure (dashed gray outlines), the position of complex III_2 varies by a clockwise rotation up to 28° relative to complex I (24). In the subtomogram averages (red outline) complex III_2 matches the predominant position of complex III_2 in single-particle structures (gray outlines) but is displaced by 8 Å away from the matrix arm (red arrows). Complex IV_1 assumes a number of different positions in the single-particle maps (thin light-green outlines), ranging from tight interactions with III_2 and I_1 to loose interactions with complex I only. Complex IV in the subtomogram average map (solid green line) correlates with the loose conformation (orange outline) (25). (Scale bar: 5 nm.)

Fig. S5. Contacts of complex IV to complex I and complex III$_2$. (*Top*) Subtomogram averages of bovine I$_1$III$_2$IV$_{ab}$ and *Y. lipolytica* I$_1$III$_2$IV$_{cd}$ supercomplexes with fitted atomic models. Cyan ellipses: contacts between complex IV and III$_2$; orange circles: contacts between complexes IV and I. (*Bottom*) Atomic models of complex I (*Left*), complex IV (*Center*), and complex III$_2$ (*Right*) with interacting helices highlighted in different colors. Cox7A and Cox8B of complex IV may interact with QCR9 of complex III and adjacent loops (cyan arrow). CX7A1 faces a helix of subunit ND5 or NUEM in complex I (orange arrow).

Fig. S6. Contacts between complex III and complex I. (*A*) Atomic models of complex I (PDB ID code 5GUP) and complex III$_2$ (PDB ID code 1BCC) fitted to the subtomogram average of the bovine I$_1$III$_2$ supercomplex. One main contact on the matrix side (cyan circle) involves subunit B22 of complex I$_1$ and subunit QCR8 of complex III$_2$. The contact on the luminal side (red circle) involves subunit B14.7 of complex I and subunit QCR8 of complex III$_2$. (*B*) Atomic model of complex III$_2$ (PDB ID code 1BCC) (10) showing subunits (shades of green) interacting with complex I. (*C*) Atomic model of complex I (PDB ID code 5GUP) indicating subunits (purple, pink) interacting with complex III$_2$. The position of the lipid bilayer is indicated by bold dashed lines. (Scale bar: 5 nm.)
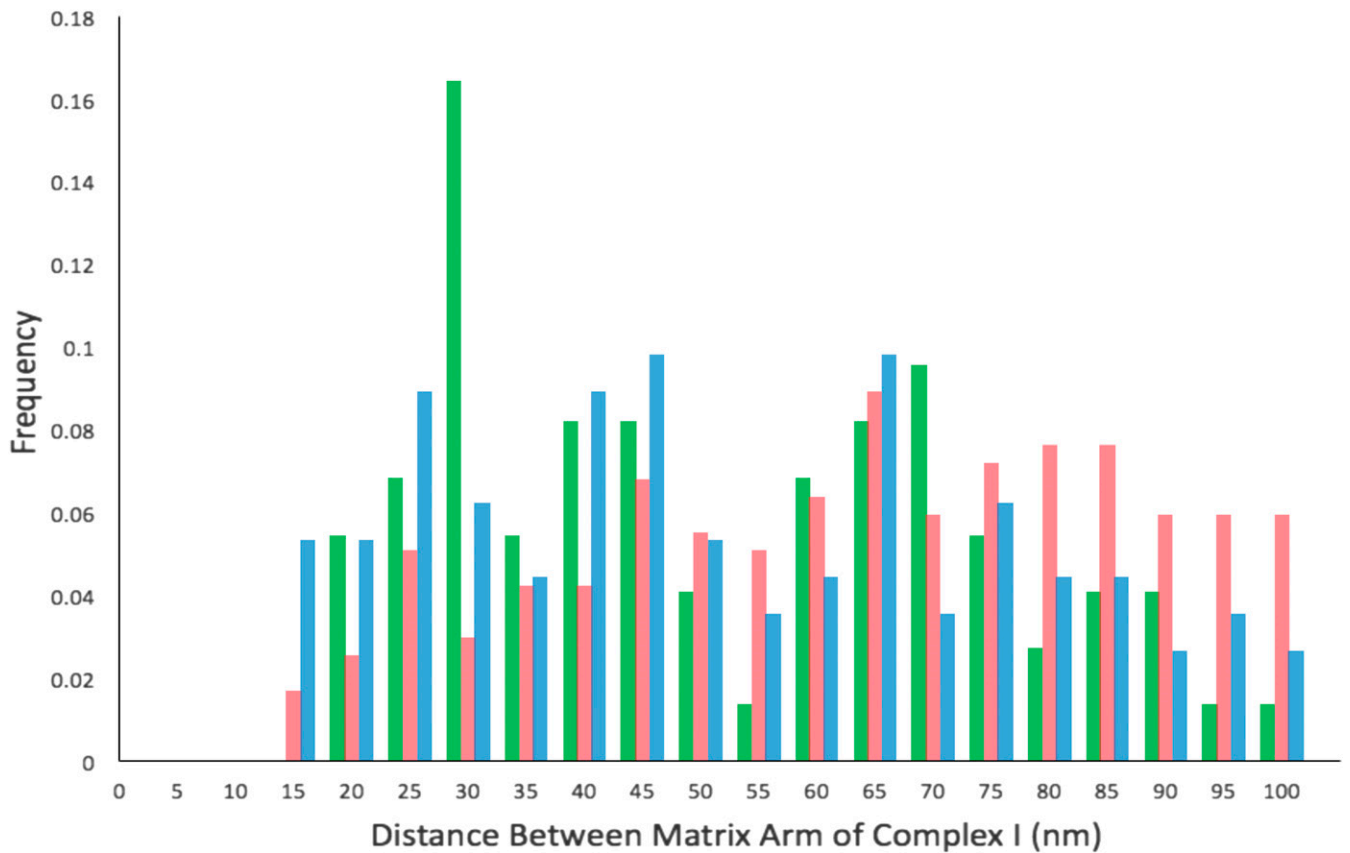
Fig. S7. Histograms of complex I matrix arm distances in situ. Distances between matrix arms of different copies of complex I in the inner mitochondrial membranes (bovine, pink; *Y. lipolytica*, blue; *A. officinalis*, green). Distances in 5-nm bins were normalized to indicate how often they were observed. For bovine heart, 235 distances were measured: 112 for *Yarrowia* and 73 for *Asparagus*. The minimum observed distance was 12 nm. Distances beyond 100 nm were not included. The distance between matrix arms in bovine and *Y. lipolytica* supercomplexes is random, whereas the *A. officinalis* distance distribution appears to peak at 28 nm (average of 12 measurements). Due to statistical uncertainty it is not possible to say whether the peak indicates a preferred distance between the plant supercomplexes in the membrane, although we cannot rule it out.

Fig. S8. Resolution estimates of subtomogram averages. Fourier Shell Correlation (FSC) of half-sets separated after alignment indicated resolutions of 36 Å for supercomplex $I_1III_2IV_{cd}$ of *Y. lipolytica* (solid blue), 39 Å for bovine $I_1III_2IV_a$ (solid red), and 43 Å for *A. officinalis* I_1III_2CA (solid green). To assess mask bias, half-maps created from tomograms were correlated with phases beyond 60 Å randomized (dashed lines). The correlation drops at the resolution at which the phases were randomized, indicating that the mask does not affect the resolution estimate (red, bovine; blue, *Y. lipolytica*; green, *A. officinalis*).